Bernhard Eidel
Ruhr-Universität-Bochum, Interdisciplinary Centre for Advanced Materials Simulation (ICAMS), Bochum, Germany

Coupling atomistic accuracy with continuum effectivity for predictive simulations in materials research – the Quasicontinuum Method

In this article we present a comparative analysis of different versions of the quasicontinuum method, which aim at a seamless transition from the atomistic to the continuum description of crystalline solids at zero temperature. All versions of this popular and powerful method exhibit the same building blocks, namely (i) a coarse-graining of fully atomistic resolution via kinematic constraints, (ii) an approximation of the energy/forces in coarse-grained regions via numerical quadrature and (iii) adaptive mesh refinement. The quasicontinuum versions are assessed in an example where a Lomer dislocation dipole is subject to shear deformation. In a second example, the fully nonlocal quasicontinuum method is used to simulate nanoindentation into an fcc single crystal. Compared with lattice statics good agreement is achieved with respect to significant details of the material behaviour for a small fraction of the computational costs.

Keywords: Multiscale modelling; Quasicontinuum; Nanoindentation; Dislocation microstructure; Surface effects

1. Introduction

Nearly 100 years have passed since John Milikan's experiment that determined the charge of an electron and – again in 1910 – the experimental proof by Ernest Rutherford of the existence of atomic nuclei. These and other fundamental insights into atomic matter have set off an avalanche of research, that has changed the world. One of the great many, lasting impacts is that in the past decade experiments on the atomic level are no longer exclusively performed in real laboratories, but equally and routinely are done in numerical laboratories. There, molecular models and simulation methods have long been an integral part for analyses in solid state physics and materials science.

Despite the considerable achievements by means of molecular simulations, which have been sped up by the ever more increasing computer power, the range of applicability of atomistic models and methods is still rather limited in that they have not yet reached the typical time and length scales of engineering applications. The reason is that quite disparate time and length scales have to be considered; for molecular dynamics the maximum time step is dictated by the frequency of thermal vibrations, hence of the order of femtoseconds, whereas a process such as, for example, crack propagation typically occurs on the order of milliseconds. The spatial problem is not less demanding, since the length scale at the bottom is in the range of atomic spacings, hence of nanometres, whereas the world of engineering problems start in the range of some centimetres – and beyond. For that reason many efforts have been undertaken to overcome the time scale and length scale dilemma by *coarse-graining* approaches. The accurate, at best *seamless* information passing from a bottom scale to a corresponding coarse-grained scale – and eventually backwards – is one of the key challenges in computational materials science.

In this paper we analyse the *quasicontinuum (QC) method* which is the most influential ambassador of the class of bottom-up, concurrent multiscale methods, that perform a coarse-graining in space at zero temperature. For the description of other methods in this family we refer to the original literature [1–5], and for reviews to [6] and [7].

Beyond some differences, which will be analysed in this article, the versions of the QC method consist of the following common building blocks:

(i) a *coarse-graining* of fully atomistic resolution via kinematic constraints in order to reduce the number of degrees of freedom. Accuracy of fully atomistic resolution is retained where necessary, the effectivity of coarse-graining is chosen where possible.
(ii) an *approximation of the energy/forces in coarse-grained regions* via numerical quadrature, which avoids the explicit computation of the site energy of each and every atom.
(iii) *adaptivity*, i.e. spatially adaptive resolution, is necessary to automatically balance accuracy and efficiency and must be directed by a suitable refinement indicator.

The three versions of the QC method are first, the original version based on Cauchy–Born elasticity as brought forth by Tadmor, Ortiz and Phillips [8], [9] and extended by contributions from Miller, Shenoy and Rodney [10]. A second, fully nonlocal version was proposed by Knap and Ortiz [11], which is the precursor of the third variant proposed in [12].

2. The Quasicontinuum-Method based on the Cauchy–Born Rule

To set the stage, we consider a crystal in d-dimensional space consisting of a set $\mathscr{L} \subset \mathbb{Z}^d$ of atoms, that are initially located on a Bravais lattice spanned by lattice vectors $\boldsymbol{A}_1, \ldots \boldsymbol{A}_d$. Their coordinates in the initial configuration read $\boldsymbol{X}_l = \sum_{i=1}^{d} l^{(i)} \boldsymbol{A}_i$, $\boldsymbol{l} \in \mathscr{L} \subset \mathbb{Z}^d$. The corresponding atomic coordinates in the current configuration are denoted by vector $\boldsymbol{x}_l$.

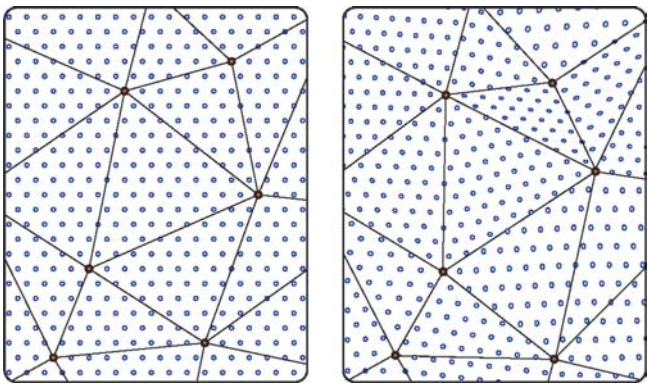

Fig. 1. Finite-element discretisation in the QC method of a crystal in the (left) undeformed and in the (right) deformed state. Atoms within elements smoothly follow the deformation of the representative atoms (mesh nodes) by linear interpolation.

2.1. Upscaling via coarse-graining

In regions of weakly varying elastic deformation it is sufficient to consider the movement of some judiciously selected *representative* atoms (rep-atoms), $\mathscr{L}_h \subset \mathscr{L}$. Only these atoms keep their independent degrees of freedom, whereas all other atoms, $\overline{\mathscr{L}_h} = \mathscr{L}/\mathscr{L}_h$, are forced to follow via kinematic constraints borrowed from the finite element method, $\boldsymbol{x}_l = \sum_{j\in\mathscr{L}_h} \boldsymbol{x}_j \varphi_j(\boldsymbol{X}_l)$, $\boldsymbol{l} \in \overline{\mathscr{L}_h}$. FE shape functions, $\varphi_{j\in\mathscr{L}_h}$, exhibit the properties, $\sum_{j\in\mathscr{L}_h}(\boldsymbol{X}_i) = 1 \;\forall\, \boldsymbol{i} \in \mathscr{L}$ (partition of unity), and, $\varphi_j(\boldsymbol{X}_{j'}) = \delta_{jj'} \;\forall\, \boldsymbol{j}, \boldsymbol{j}' \in \mathscr{L}$ (compact support). The use of (here: linear) shape functions for interpolation requires the generation of a triangulation with representative atoms as mesh nodes. Figure 1 schematically displays the discretisation of the crystal into finite elements.

Of course, the interpolation of nodal displacements implicitly introduces a continuum assumption into the QC method. Notwithstanding, this first approximation is purely kinematical in nature, no constitutive assumption is made.

This approximation step of coarse-graining reduces the number of independent degrees of freedom for the calculation of the exact total potential $E^{\mathrm{tot}}(\{\boldsymbol{x}_i | \boldsymbol{i} \in \mathscr{L}\}) \rightarrow E^{\mathrm{tot}}(\{\boldsymbol{x}_i | \boldsymbol{i} \in \mathscr{L}_h\}) =: E^{\mathrm{tot},h}$ and thus reduces the number of unknowns in the computation.

Both existing QC methods have this approximation step of (finite element) discretisation in common, but differ in the way further approximations are made. Next, we focus on the QC version based on Cauchy-Born elasticity, in Section 3 the fully nonlocal QC versions are described.

2.2. Efficient energy/force calculation: the local QC

After thinning-out dispensable degrees of freedom via linear finite-element shape functions, i. e. approximation (i), the first QC-version accomplishes an efficient energy/force calculation in the continuum region by recourse to the so-called *Cauchy–Born Rule*, hence QC-CBR, resulting in what is referred to as the *local* formulation of the QC.

The CBR postulates that when a monatomic crystal is subjected to a small linear displacement of its boundary, then all atoms will follow this displacement, see [13–15]. This is illustrated in Fig. 2 for the deformation $\varphi : \Omega \rightarrow \mathbb{R}^3$ of a crystalline cantilever undergoing elastic bending with a deformation gradient $\boldsymbol{F} = \partial_{\boldsymbol{X}}\varphi(\boldsymbol{X})$ and a Jacobian

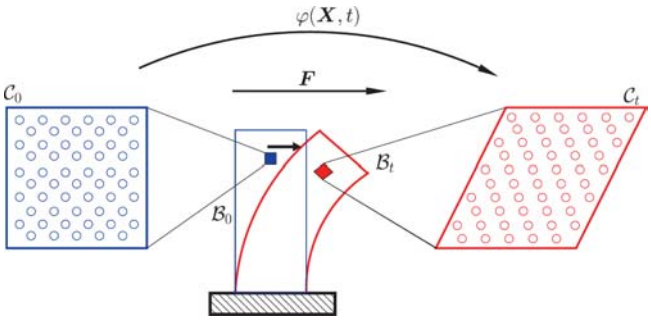

Fig. 2. Schematic representation of the CBR assuming a homogeneous deformation state in small volumes.

$J = \det \boldsymbol{F} > 0$, where $\boldsymbol{X}$ designates a material point in the reference configuration.

This is applied within the QC-CBR in that a – locally – uniform deformation gradient at the continuum or macroscale is directly mapped to the same *uniform* deformation on the atomistic or nano-scale. For crystalline solids with a simple lattice structure the assumption of locally homogeneous deformation state implies that every atom in a region subject to a uniform deformation gradient will be energetically equivalent. As a consequence, the calculation of the energy for a specific finite element can be approximated by computing the energy of only a single atom in the deformed state and multiplying this figure by the number of atoms in the specific finite element. Within the QC-computational framework, the calculation of the CB energy is done separately in a subroutine; for a given deformation gradient $\boldsymbol{F}$ the lattice vectors in a unit cell with periodic boundary conditions is deformed according to $\boldsymbol{F}$

$$\boldsymbol{a}_i = \boldsymbol{F}\boldsymbol{A}_i \tag{1}$$

where $\boldsymbol{A}_i$ and $\boldsymbol{a}_i$ are the lattice vectors in the undeformed configuration and in the deformed configuration, respectively. The deformed lattice vectors enter the employed potential for energy calculation, such that the CBR enables the free energy of a crystalline body (as a function of lattice vectors) in its deformed configuration to be expressed alternatively as a function of the deformation gradient $\boldsymbol{F}$. The corresponding strain energy density in the element is then given by

$$\mathcal{E} = \frac{E_0(\boldsymbol{F})}{\Omega_0} \tag{2}$$

where Ω_0 is the unit cell volume (in the reference configuration) and E_0 is the energy of the unit cell when its lattice vectors are distorted according to $\boldsymbol{F}$. Now the total energy of a finite element is this energy density times the element volume, the total energy of the problem is simply the sum of all element energies:

$$E^{\mathrm{tot},h} = \sum_{i=1}^{N_{\mathrm{element}}} \Omega_i \, \mathcal{E}(\boldsymbol{F}_i) \tag{3}$$

where Ω_i is the volume of element i.

Linear interpolation functions in tetrahedral finite elements require only one single Gauss-point for numerical quadrature and therefore imply a constant deformation gradient $\boldsymbol{F}$ per element as visualised in the right of Fig. 1. As a consequence, the application of the CBR implies that in the

energy calculation the summation over the number of lattice sites N boils down to the number of finite elements N_{element}, see Eq. (3).

Since the crystal is in general subject to inhomogeneous deformations, the element-wise constant deformation gradient is an approximation and so is the calculated energy via the CBR. In settings where the deformation is varying slowly and the element size is adequate with respect to the variations of the deformation, this type of energy calculation is sufficiently accurate and very effective.

An analysis on the range of validity of the CBR can be found in [16] and in [17] where it turns out in the latter reference that the CBR fails for relatively small elastic deformations. An extension of the classical linear CBR to second order is proposed in [18].

2.3. Nonlocal QC

In nonlocal regions, which can be eventually refined to fully atomistic resolution, the energy of the atoms residing on a mesh node (representative atom) is calculated. Specifically, the new approximate energy takes the form

$$E^{\text{tot},h} = \sum_{\alpha=1}^{N_{\text{rep}}} n_\alpha \, E_\alpha \left(\boldsymbol{u}_h\right) \tag{4}$$

The computational saving is that the summation of all the atoms is replaced by a sum over all representative atoms N_{rep}. In the line of numerical quadrature, n_α is the weight function for rep-atom α which requires for consistency

$$\sum_{\alpha=1}^{N_{\text{rep}}} n_\alpha = N \tag{5}$$

Hence, n_α is the number of atoms represented by atom α, which implies in the limiting case of fully atomistic resolution $n_\alpha = 1$.

2.4. Mixed Local–Nonlocal QC

Since the nonlocal QC is employed in regions where atomic scale accuracy is needed, while the local QC has the advantage of computational efficiency in regions where the deformation is changing relatively slowly on the atomic scale, a scheme is favourable that uses both formulations concurrently in a single simulation. For that aim, a framework has been developed that combines the local QC and the the nonlocal QC as already described above.

As in the energy-based nonlocal QC, the coupled approach is based on the ansatz that the energy can be approximated by computing only the energy of the rep-atoms. In the coupled approach however, each rep-atom is judiciously selected as being either local or nonlocal depending on its deformation environment. Thus, the rep-atoms are divided into N_{loc} local rep-atoms and N_{nonloc} nonlocal rep-atoms ($N_{\text{loc}} + N_{\text{nonloc}} = N_{\text{rep}}$). Doing this, the total energy is approximated as

$$E^{\text{tot},h} = \sum_{\alpha=1}^{N_{\text{nonloc}}} n_\alpha \, E_\alpha \left(\boldsymbol{u}_h\right) + \sum_{\alpha=1}^{N_{\text{loc}}} n_\alpha \, E_\alpha \left(\boldsymbol{u}_h\right) \tag{6}$$

The weights n_α for each rep-atom (local or nonlocal) are determined from a tessellation that divides the body into cells around each rep-atom. The numerically expensive Voronoi tessellation can be replaced by an approximate Voronoi diagram. The Voronoi cell of rep-atom α contains a total of n_α atoms. Of these atoms, n_α^i reside in element i adjacent to rep-atom α. The total weighted energy contribution of rep-atom α is then calculated by use of the CBR within each element adjacent to α, hence

$$n_\alpha E_\alpha = \sum_{i=1}^{M} n_\alpha^i \, \Omega_0 \, \mathcal{E}\left(\boldsymbol{F}_i\right) \qquad n_\alpha = \sum_{i=1}^{M} n_\alpha^i \tag{7}$$

where $\mathcal{E}$ is the energy density in element i by the CBR, Ω_0 is the Wigner–Seitz volume of a single atom and M is the number of elements adjacent to α.

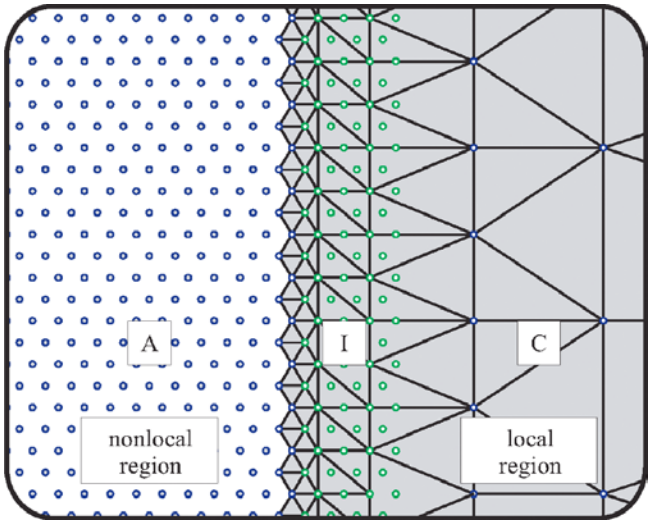

Fig. 3. The scale transition scheme in the QC-CBR, where the nonlocal region (A) overlaps in the interface zone (I) with the local continuum region (C), which is discretised with finite elements and subject to the CBR.

2.5. The ghost-force problem

The first version of the QC inherently exhibits *ghost forces*, defined as spurious forces arising at the interface between local and nonlocal regions, see Fig. 3. These forces thus follow from the duality in atomic interactions, where the motion of representative atoms (i.e. finite element nodes) in the local region subject to CBR will affect the energy of nonlocal representative atoms, while the converse may not be true.

There are two different concepts to reduce ghost forces in QC-CBR:

1. correction by applying a *static correction force field*, see [10].
2. correction by *continuation*, see [16] and [19].

The first remedy against ghost forces is to introduce static correction forces, which exhibit the drawback that they are not derivable from a "correction potential energy", i.e., they are nonconservative, see [10]. This may lead to serious problems with energy conservation during a molecular-dynamics simulation, as reported in [19]. In order to cure the problem of *ghost forces* without new shortcomings, this reference introduces a buffer layer between the two regions of space, where atoms are subject to specific rules concerning how they interact with their local and nonlocal neigh-

bourhood. In a similar spirit is the contribution of [16], where the approach of local reconstruction schemes is generalised.

3. The fully nonlocal, cluster-based Quasicontinuum-Method

A fully nonlocal QC-version as proposed by Knap and Ortiz in 2001, [11], aims to overcome the aforementioned force mismatch between local and nonlocal regions in QC-CBR. For that aim they replace the CBR by a nonlocal theory to be described and hence avoid incompatibilities of different physical descriptions at discrete interfaces. The scale transition in the fully nonlocal QC is realized in a more continuous manner by gradual coarse-graining, enabling a seamless scale transition, see Fig. 4., whereas in QC-CBR the scale transition is at the discrete interface where local Cauchy–Born elasticity as the continuum constitutive model meets nonlocal atomistics, see Fig. 3. In the above structure of the QC building blocks in Section 1, properties (i)–(iii), fully nonlocal QC versions introduce for property (ii) the use of summation rules for the sampling of *forces* or the *energies* in spherical clusters, which can be seen as representative crystallites.

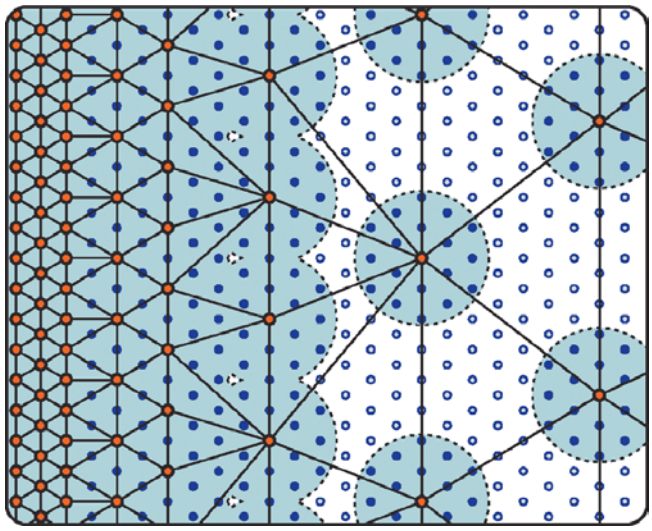

Fig. 4. The scale transition scheme in fully nonlocal QC-versions based on force/energy sampling in spherical clusters: the atomistic-continuum coupling is realised in a continuous manner by gradual coarse-graining enabling a seamless scale transition.

3.1. Sampling of energy/forces in spherical clusters

Even after coarse-graining, the total energy still depends on the site energy E_k of each and every atom $\boldsymbol{k}$, $E^{\mathrm{tot},h} = \sum_{k\in\mathscr{L}} E_k$. Due to the prohibitive computational expense of this task, a second approximation becomes necessary, which is again, like discretisation, a very standard in classical finite element methods: numerical quadrature.

For that purpose [11] proposed to perform force evaluations no longer at each lattice site in the crystal but to restrict them to sampling clusters. These sampling clusters $\mathscr{C}_i$ are spheres of radius R_c and are chosen to have a mesh node in its centre, see Fig. 5. Hence, they are defined as $\mathscr{C}_i = \{\boldsymbol{k} : |\boldsymbol{X}_k - \boldsymbol{X}_i| \leq R_c(\boldsymbol{i})\}$. Note that the sampling clusters may have different positions, e. g. in the interior of the finite element.

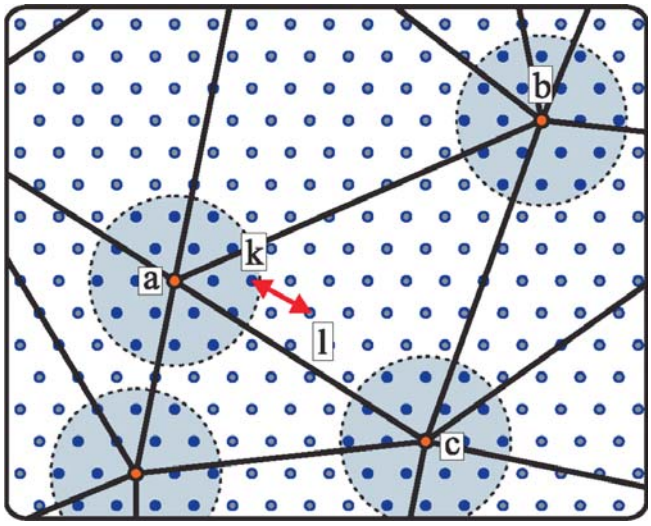

Fig. 5. Spherical clusters around mesh nodes for the explicit sampling of forces or energies. The interaction of sampling atom $\boldsymbol{k}$ inside the cluster with non-sampling atom $\boldsymbol{l}$ outside the cluster must be symmetric to fulfill Newton's third law.

Assuming a pair potential $V = V(|\boldsymbol{r}_{kl}|)$ with $\boldsymbol{r}_{kl} = \boldsymbol{x}_k - \boldsymbol{x}_l$ and omitting here and in the following the contribution of an external potential V^{ext}, the force acting on node $\boldsymbol{a}$ reads for **force sampling** in the cluster

$$\begin{aligned} \boldsymbol{f}_a^h &= \sum_{i\in\mathscr{L}_h} n_i \sum_{k\in\mathscr{C}_i} \boldsymbol{f}_k \varphi_a(\boldsymbol{X}_k) \\ &= -\sum_{i\in\mathscr{L}_h} n_i \sum_{k\in\mathscr{C}_i} \left[\sum_{l\in\mathscr{L}} V'(|\boldsymbol{r}_{kl}|) \frac{\boldsymbol{r}_{kl}}{|\boldsymbol{r}_{kl}|} \right] \varphi_a(\boldsymbol{X}_k) \end{aligned} \tag{8}$$

The equilibrium configurations of interest are the minimisers of $E^{\mathrm{tot},h}$, i. e. the solutions of the variational problem:

$$\min_{\{x_a\}} E^{\mathrm{tot},h} \rightarrow \boldsymbol{f}_a^h = \boldsymbol{0} \quad \forall\, \boldsymbol{a} \in \mathscr{L}_h \tag{9}$$

Energy minimisation physically corresponds to solving for the configuration for which at every mesh node $\boldsymbol{a}$ the sum of forces on each degree of freedom is zero. Based on this fact, Knap and Ortiz [11] search for the equilibrium by directly working from an approximate expression for the forces according to Eq. (8) rather than working from the explicit differentiation of a total energy functional.

In [12] however, we introduced the sampling at the energy level, thus

$$E^{\mathrm{QC}} = \sum_{i\in\mathscr{L}_h} n_i \sum_{k\in\mathscr{C}_i} E_k \approx E^{\mathrm{tot},h} \tag{10}$$

The counterpart to Eq. (8) yields for energy sampling

$$\begin{aligned} \boldsymbol{f}_a^h &= -\frac{\partial E^{\mathrm{QC}}}{\partial \boldsymbol{x}_a} = \sum_{i\in\mathscr{L}_h} n_i \sum_{k\in\mathscr{C}_i} \\ &\cdot \frac{1}{2} \sum_{l\in\mathscr{L}} \left[V'(|\boldsymbol{r}_{kl}|) \frac{\boldsymbol{r}_{kl}}{|\boldsymbol{r}_{kl}|} [\varphi_a(\boldsymbol{X}_k) - \varphi_a(\boldsymbol{X}_l)] \right] \end{aligned} \tag{11}$$

It is worth noting that for energy sampling – as opposed to force sampling – the force expression $\boldsymbol{f}_a^h$ in Eq. (11) is explicitly derived from a well defined total potential E^{QC},

Eq. (10). The analysis in [12] brought forth that the stiffness matrix derived from the force expression in Eq. (8) is nonsymmetric, thus indicating that the forces are not conservative. Hence, for force sampling the variational structure is lost.

This result was the motivation in [12] to introduce the sampling at the energy level as described in Eq. (10), which endows the fully nonlocal QC theory with a variational structure, since the consistently derived forces are conservative as indicated by symmetric stiffness matrices. For a detailed analysis we refer to [12].

The cluster based QC variants are abbreviated according to the sampled quantity, as CQC-F for force sampling, and as CQC-E for energy sampling.

Cluster weights. In both cases, i.e. for force and energy sampling, factor n_i is the weighting of the force/energy contribution of cluster $\mathscr{C}_i$. The cluster weights $n_i, \boldsymbol{i} \in \mathscr{L}_h$, are calculated under the requirement that the summation over all linear interpolation functions must be exact, see [11], hence

$$\sum_{i\in\mathscr{L}_h} n_i \sum_{k\in\mathscr{C}_i} \varphi_j(\boldsymbol{X}_k) = \sum_{k\in\mathscr{L}} \varphi_j(\boldsymbol{X}_k) \quad \forall \quad \boldsymbol{j} \in \mathscr{L}_h \tag{12}$$

The calculation of the weights implies the assumption that the quantity subject to sampling can be exactly approximated if it is linear between the mesh nodes.

3.2. Numerical errors in CQC-E

Each of the two approximations made in the cluster based QC introduces a numerical error compared with lattice statics, which will be described for CQC-E.

(I) *Discretisation error*:

The approximation of coarse-graining, as described in Subsection 2.1. reduces the number of independent degrees of freedom for the calculation of the exact total potential

$$E^{\mathrm{tot}}(\{\boldsymbol{x}_i \mid \boldsymbol{i} \in \mathscr{L}\}) \to E^{\mathrm{tot}}(\{\boldsymbol{x}_i \mid \boldsymbol{i} \in \mathscr{L}_h\}) = E^{\mathrm{tot},h} \tag{13}$$

and thus reduces the number of unknowns in the computation. This error is reduced by adaptive mesh-refinement directed by a refinement indicator.

(II) *Error of numerical quadrature*:

(A) The energy is sampled in clusters of confined size $\mathscr{C}_i \subset \mathscr{L}$ which leads to an approximation of $E^{\mathrm{tot},h}$ by E^{QC}, see Eq. (10)

$$E^{\mathrm{tot},h} \to E^{\mathrm{QC}} \tag{14}$$

and the corresponding force error obeys the format

$$\boldsymbol{f}^* = -\mathrm{grad}\{E^{\mathrm{QC}} - E^{\mathrm{tot},h}\} \tag{15}$$

(B) Weighting factors are determined such that they are exact, only if the energy is piecewise linear, [11].

In [12] a test was designed to analyse the error in numerical quadrature. An infinite single crystal, modelled as a crystal of finite size with periodic boundary conditions, was relaxed into its equilibrium state. Since no external forces are present, the exact solution is zero displacement in the entire crystal. The key aspect of this test however is to check, if CQC based on energy sampling can achieve a *seamless* scale transition. For that aim a discretisation was chosen of fully atomistic resolution in the centre of the crystal and increasingly coarse-grained towards the border of the crystal. The result of relaxation has shown nonzero displacements as induced by spurious forces. These forces could be reduced by increasing the cluster size. In the limit, where the clusters are large enough to capture each and every atom in the crystal, the spurious forces identically vanish. This test shows that CQC-E can achieve a truly seamless scale transition.

Moreover, the test elucidates important properties of the observed residual forces, which are different from the ghost forces in QC-CBR by source and nature.

The convergence properties of the residual forces in CQC-E show that they stem from the approximation made in numerical quadrature. Ghost forces in QC-CBR follow from the incompatibility of the local and the nonlocal concept.

The aforementioned error in numerical quadrature is described in Eq. (15). It reflects that residual forces in CQC-E are conservative in nature; they are derived from a unified total potential and as a consequence, they are symmetric. Ghost forces in QC-CBR however are not conservative, since they do not derive from a unified potential and consequently, they are not symmetric, i.e. the motion of rep-atoms in the local region subject to CBR will affect the energy of nonlocal rep-atoms, while the converse may not be true.

Moreover, Eq. (15) reflects the inherent property of CQC-E to estimate the error in numerical quadrature with arbitrary accuracy. This can be easily done by calculating the energy twice, but the second time with a larger cluster size which gives an improved energy approximation.

Summarising, the fully nonlocal cluster QC based on energy sampling exhibits advantages compared to its precursor based on force sampling: CQC-E preserves the variational structure of lattice statics leading to conservative forces as indicated by symmetric stiffness matrices. More specifically, energy sampling implies the strict symmetry of atomic interactions in all regions, even across the boundary of clusters, whereas force sampling does not in general. Energy sampling also exhibits some numerical advantages. Standard algorithms for the numerical minimisation of functionals such as CG methods can directly be applied, since they generally require gradients as well as evaluations of the functional (the energy) itself. Moreover, a minimiser can be found if the energy exhibits a minimum.

4. Numerical examples

4.1. Dipole of Lomer dislocations subject to shear force

In this test set, as recently proposed in [7], we will compare the performance of the versions of the QC method (QC-CBR and CQC-E) against fully atomistic lattice statics as reference solution. The test is a block of single crystalline aluminium with a dipole of Lomer dislocations in its centre, which is subject to increasing shear strain $\gamma = 0 - 0.057$, cf. Fig. 6. When the block is increasingly sheared, Peach–Koehler forces build up and, when large enough, drive the two dislocation cores into opposite directions. The crystal is approximately 400 Å × 400 Å in the X–Y plane and periodic in Z (with a periodic length of 2.85 Å). Since the lattice constant for this model of aluminium is 4.032 Å, this region contains 27760 atoms. The mesh used for the QC simulations is displayed in Fig. 7. A small band of thickness T is refined to fully atomistic resolution, namely for $Y = \pm T$ Å. Here, we consider $T = 10, 20$ Å. The Lomer di-

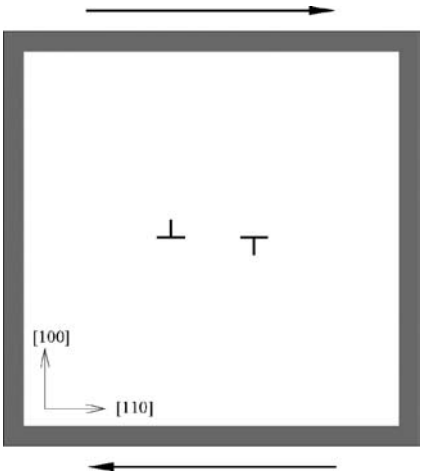

Fig. 6. Test set used to compare the versions of the QC methods. A Lomer dipole, 40 Å wide, is centred in the model. The dark frame around the edges of the model is held fixed to various levels of applied shear strain to force the dislocations to move.

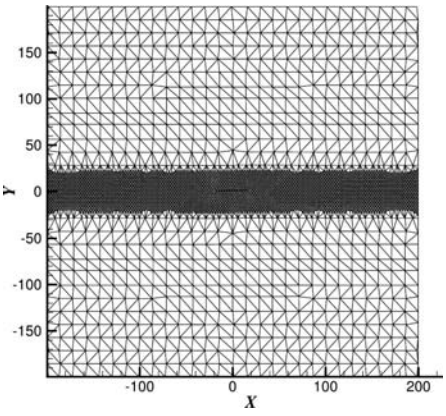

Fig. 7. Finite-element mesh for the Lomer dipole.

pole lies on the $Y = 0$ plane, with the two cores initially located at $X \approx \pm 20$ Å.

The accuracy of the QC methods against lattice statics are measured using two physically meaningful criteria. First, the dislocation motion is tracked in terms of the core spacing as a function of shear strain. Second, the shear force is recorded as a function of the shear strain, which includes the sudden change in the force when the dislocations start to move for sufficiently large Peach–Koehler forces.

In [7] the displacement error in the initial relaxation ($\gamma = 0$) is used as a measure for the intended *smooth* scale transition between the fully atomistic core region and the coarse-grained finite element region. Hence the local error for atom α is calculated according to

$$e^{\alpha} = ||\boldsymbol{u}^{\alpha}_{qc} - \boldsymbol{u}^{\alpha}_{ex}|| \tag{16}$$

where $\boldsymbol{u}^{\alpha}_{qc}$ and $\boldsymbol{u}^{\alpha}_{ex}$ are the displacements of atom α in the QC simulation and lattice statics calculation, respectively.

Initial relaxation. The displacements and the corresponding displacement error e^{α} after the initial relaxation of the crystal are reported in Figs. 8 and 9. Focussing on the region influenced by the dislocation dipole, as displayed in Fig. 8, we observe within the strip of fully atomistic resolution an excellent agreement with lattice statics for CQC-E with 13 sampling atoms per cluster, see Fig. 9. Only in a narrow band right along the atomistic strip there is a visible error, which for CQC-E is throughout smaller than 0.14 Å. For QC-CBR (with ghost force correction, hence GFC) the error is throughout even smaller, $e^{\alpha} < 0.03$ Å. In the fully atomistic strip close to the dislocation dipole, the error is somewhat larger than in CQC-E.

Note that the loading and boundary conditions according [7], see Fig. 6, enforce the quasi-uniform deformation of simple shear in some distance to the dislocation cores. This is obviously the *best* case for QC-CBR, since the CBR by its very construction assumes a uniform deformation state.

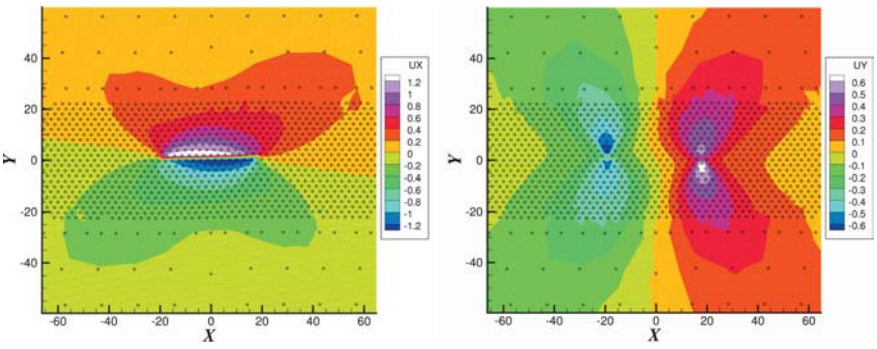

Fig. 8. Displacements in (left) X- and (right) Y-direction (Å) during initial relaxation ($\gamma = 0$) for CQC-E with 13 sampling atoms, strip width $T = 20$ Å.

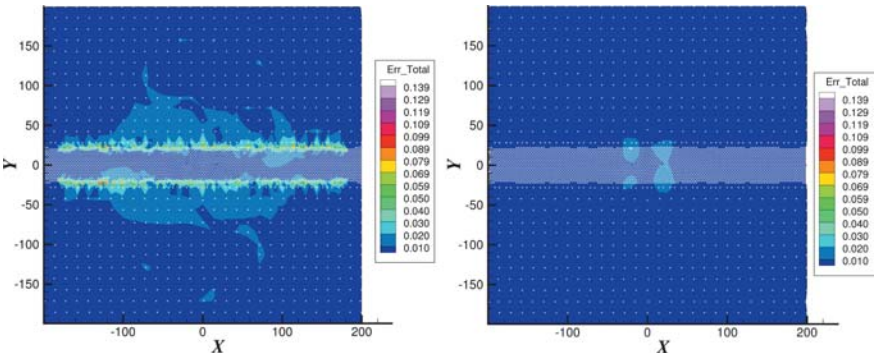

Fig. 9. Distribution of the displacement error e^{α} (Å) according to Eq. (16) for (left) CQC-E and for (right) QC-CBR-GFC, $T = 20$ Å.

Remarkably, this does not only apply for some elements but for the *entire crystal* in the simulation box in some distance to the dislocation cores.

Force-shear curve and dipole motion. We agree with [7] in that "*the curves for the shear load versus applied shear and core separation as a function of applied shear strain are the most interesting physical results one may like to extract*". As it will turn out, both aspects are closely connected. We start with the second relation reported in Fig. 10 and observe that both QC versions capture for various parameters the sessile behaviour of the dislocation cores in that their distance remains constant up to $\gamma \approx 0.045$. For strip width $T = 10$ Å however, the QC-CBR simulations underestimate the load level for dislocation motion which is equally reflected in the F–γ curve of Fig. 11 by a premature force-drop. For the same strip width CQC-E(13) performs better, since it predicts quite accurately the load level, where the dislocations move all at once, but the final position of the cores is quite inaccurate. For a larger strip width of $T = 20$ Å these problems are overcome; both QC versions (namely CQC-E(13)-20 and QC-20) correctly predict the load level of dislocation motion/force drop and they are in quantitative agreement with lattice statics concerning the final dislocation core spacing at $\gamma = 0.057$. The main conclusion is that the influence of dislocation cores within a finite distance, viz. Fig. 8, requires for both QC versions fully atomistic resolution in a sufficiently large neighbourhood around the defects.

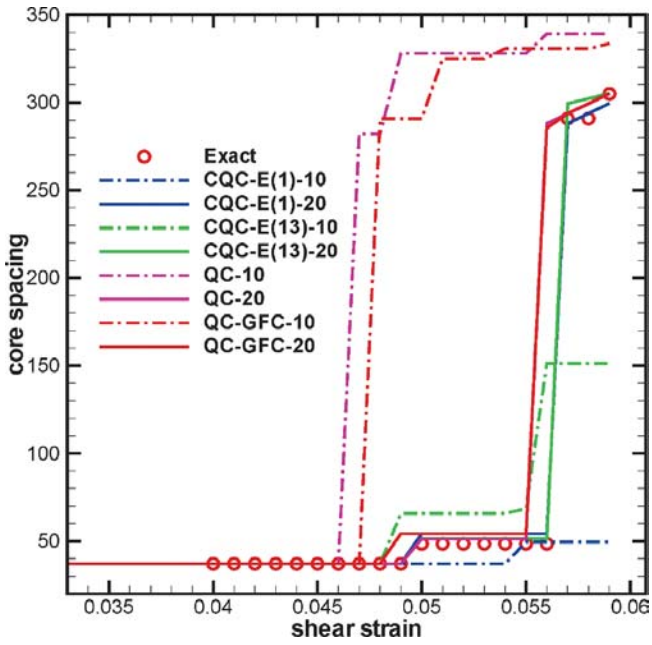

Fig. 10. Distance between the dislocation cores as a function of the applied shear strain for lattice statics, for QC-CBR and for CQC-E. Force F in (eV · Å^{-1}), strip width T as indicated.

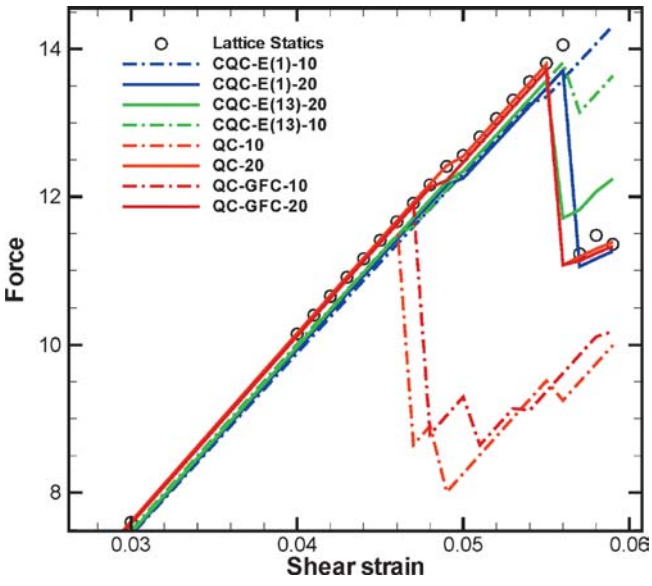

Fig. 11. Applied shear force as a function of the applied shear strain for the lattice statics simulation, for QC-CBR and for CQC-E. Force F in (eV · Å^{-1}), strip width T as indicated.

There is much merit in this benchmark test, but general conclusions on the overall performance of the QC versions cannot be drawn from one single test. This is especially true, since the test does not check at least two important features, which versatile and powerful concurrent multiscale method must provide.

(A) *Adaptive spatial resolution* in order to keep track of defect evolution like dislocation motion or crack growth by way of automatic, local mesh-refinement – or eventually mesh-coarsening. This feature must balance the opposite requirements of accuracy and efficiency.

(B) *Free surface effects* must be accurately described, since they cannot be neglected at the nanoscale and, naturally, every material body is finite and thus separated by free surfaces from the rest of the world.

These two features as well as other aspects of accuracy and efficiency are assessed in the next example, where the fully nonlocal 3D software framework for CQC-E, as proposed in [12], is used for the simulation of nanoindentation.

4.2. Nanoindentation into (001) fcc aluminium

Nanoindentation is a paradigmatic problem for concurrent multiscale modelling and is of some relevance in materials science. The simulation results will be validated by comparison with lattice statics, which is the QC method's fully atomistic counterpart. In this comparison we focus on the criteria *efficiency* and *accuracy*. For that aim we measure free surface effects and record the characteristic force–depth (F–h) curve, from the elastic branch up to dislocation nucleation and beyond. Finally, we compare the evolution of dislocation microstructure which assesses adaptive mesh-refinement.

The material under consideration is fcc single crystalline aluminium. The computational box adopted in the computations comprises $64 \times 64 \times 64$ Bravais-lattice cells. Atoms on the lateral faces of the box are fixed in normal direction to the faces, atoms at the bottom are fixed in z-direction but free to move within the bottom plane. In Fig. 12 the axes of the coordinate system correspond to <001> directions. A spherical indenter of radius R is modelled as an external potential V^{ext} of the form

$$V^{\text{ext}}(\boldsymbol{x}) = A \cdot \theta(R - r) \cdot (R - r)^3, \quad r = |\boldsymbol{x} - \boldsymbol{c}| \qquad (17)$$

where parameter A represents the strength of the repulsive force, $\theta(r)$ the step function, R the indenter radius and $\boldsymbol{c}$ denotes the position of the midpoint of the indentor. In the simulations the values $A = 2000$ eV Å^{-3} and $R = 16\,a_0$ with lat-

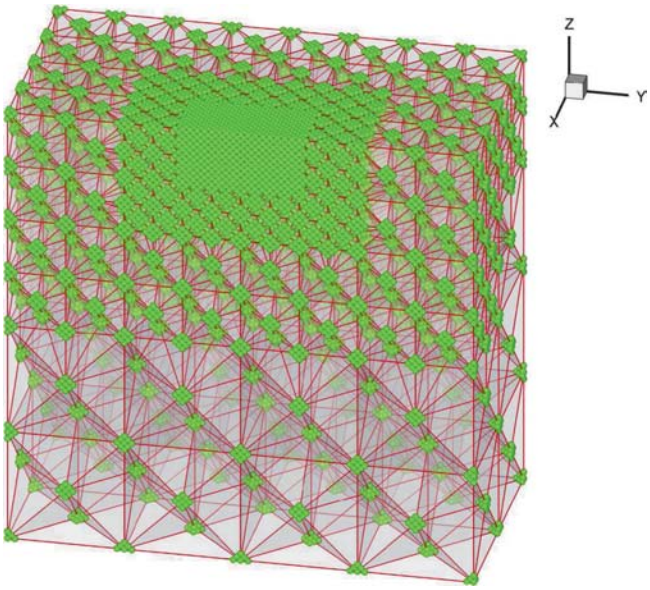

Fig. 12. Cross-sectional view of the initial mesh for the CQC-E simulation. The mesh nodes are encircled by atomic clusters in green.

tice constant $a_0 = 4.032$ are used. The energy of the crystal is modelled using the Embedded Atom Method (EAM) potential. The ball indenter is driven into the [001] oriented single crystal in small displacement increments Δh, where at each loading step a new stable equilibrium configuration of the system is found by a nonlinear version of the conjugate gradient method.

4.2.1. Surface effects

The very first step in the simulation is an initial relaxation, where the indentor's force is not yet present. Hence, the crystal's equilibrium configuration is mainly influenced by the effect of free surfaces.

Since surface atoms exhibit a smaller coordination number compared with bulk atoms, the bonding to their neighbours is stronger, the relaxed lattice distances are smaller.

CQC-E simulations of the initial relaxation are performed on the mesh in Fig. 12. For the cluster radius two different values are chosen in distinct computations; first $R_c = 1\,a_0$ corresponding to 18 sampling atoms per cluster, second $R_c = 2\sqrt{2}\,a_0$ with 381 atoms per cluster. Figure 13 displays the relaxation displacements in z-direction for CQC-E with $R_c = 2\sqrt{2}\,a_0$ and for lattice statics. When the cluster contains only 18 atoms, the shrinkage in z-direction at the cube's corner is $u_z = -3.3$ Å, which is considerably larger than that one of lattice statics, $u_z = -1.3$ Å. For a sufficiently large $R_c = 2\sqrt{2}\,a_0$ however, $u_z = -1.1$ Å is very close to the reference value of lattice statics.

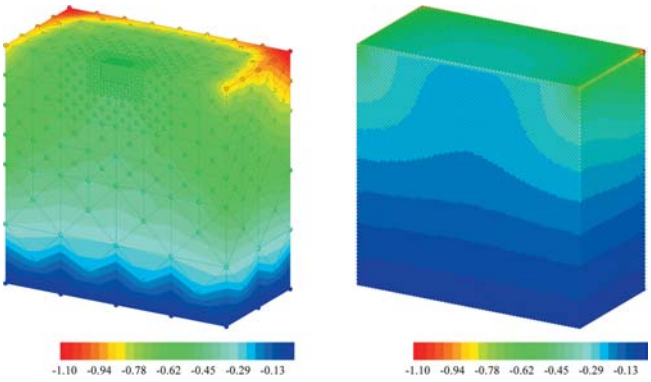

Fig. 13. Displacement component u_z (Å) in thickness direction in the initial relaxation for (left) CQC-E ($R_c = 2\sqrt{2}a_0$) and for (right) lattice statics.

Hence, for an already moderately large cluster size, CQC-E can accurately account for relaxation effects at free surfaces. Since this holds even in coarse-grained regions such as in the corners of the cubic sample where relaxation is maximum, the method effectively overcomes the necessity to choose fully atomistic resolution at free surfaces.

The reason for this is that CQC-E is fully nonlocal everywhere along with the choice to locate the sampling region around the mesh nodes and hence directly to the surface as the region of interest. For the same physical reason the QC version based on the CBR rule cannot capture surface effects by its very composition, cf. [20]. It is the assumption of *local homogeneity* inherent in the CBR which makes it blind for suchlike heterogeneous situations, where surface atoms are in fact exposed to a highly non-centrosymmetric neighbourhood. Fully atomistic resolution at free surfaces can cure this problem within the QC-CBR framework, but is computationally expensive.

The accurate description of free surface effects is a particular strength of the fully nonlocal QC method compared to other concurrent multiscale methods, which generally employ continuum – hence local – constitutive equations in the coarse-grained, i. e. finite element regions.

4.2.2. Dislocation nucleation and microstructure evolution

During the deformation process the force–displacement curve is recorded, see Fig. 14. In the first branch of purely elastic deformation the force increases continuously. When a critical value of the indenter force F is reached, the first dislocation nucleates in the single crystal. This onset of plastic deformation is marked by a discrete force drop in the F–h curve.

In the elastic branch CQC-E generally well agrees with lattice statics. Increasing the cluster size from $R_c = 1\,a_0$ to

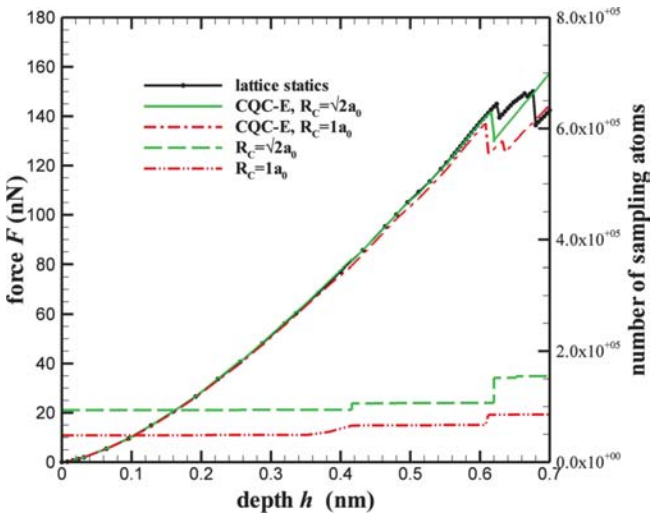

Fig. 14. Force–depth (F–h) curve in nanoindentation. Quasicontinuum (CQC-E) for various cluster sizes versus lattice statics.

$R_c = \sqrt{2}\,a_0$ already yields quantitative agreement with lattice statics.

Dislocation nucleation occurs in the CQC-E simulations for the chosen cluster radii throughout at a somewhat smaller load level than for lattice statics. Increasing the cluster size improves the approximation, for $R_c = \sqrt{2}\,a_0$ excellent agreement with the fully atomistic resolution is achieved, see Fig. 14.

The overall good accuracy of CQC-E in the F–h curve is achieved for comparatively small computational costs. For cluster radius $R_c = 1\,a_0$ the number of sampling atoms (labelled on the right vertical axis in Fig. 14) increases during adaptive refinement steps from initially approximately 48 000 to approximately 86 000, which is still only 8 % of the number of atoms used in the fully atomistic lattice statics simulation.

The QC simulation for cluster radius $R_c = 1\,a_0$ is approximately 8 times faster than lattice statics. The efficiency can be arbitrarily improved by increasing the size of the simulation box, since only large elements are added in lateral and depth direction. In contrast to lattice statics we may now safely use large simulation boxes without great loss of efficiency to eliminate any undesirable simulation size effects.

4.2.3. Adaptivity ensures undisturbed dislocation motion

Adaptivity is necessary in concurrent multiscale frameworks for a well-balanced trade-off between accuracy and efficiency. The discretisation error in the present work is reduced by an adaptive refinement strategy based on a heuristic refinement indicator $\varepsilon(K)$, which is defined according to [11] as

$$\varepsilon(K) = \sqrt{|\mathrm{II}_E(K)|} \cdot \frac{h(K)}{b} \tag{18}$$

where $\mathrm{II}_E(K)$ is the second invariant of the Green–Lagrange strain tensor $\boldsymbol{E}$ in simplex K, and $h(K)$ is the size of K. Since b denotes the length of the smallest Burgers vector for the given crystal, the criterion, though heuristic, reflects physical reasoning, since the current deformation is compared with the smallest unit of plastic deformation. Elements with $\varepsilon(K)$ larger than a tolerance are targeted for refinement.

Figure 15 displays some selected meshes as a result of adaptive mesh refinement during the indentation process. In the third and forth mesh a localisation of deformation can be seen in the core region of fully atomistic simulation, which indicates dislocation motion, first on a single, right after on a second {111} plane.

Obviously, the 3D process of dislocation nucleation and microstructure evolution remains mostly hidden behind the finite element meshes of Fig. 15. This lack of transparency is not satisfactory but equally applies to standard molecular simulations. For that purpose an indicator is necessary that detects defects and visually extracts them from their undisturbed surroundings. The so-called centro symmetry parameter, [21], meets these requirements and enables classification of characteristic defects. It is defined for each atom in an fcc crystal according to

$$P = \sum_{i=1}^{6} |\boldsymbol{r}_i + \boldsymbol{r}_{-i}|^2 \tag{19}$$

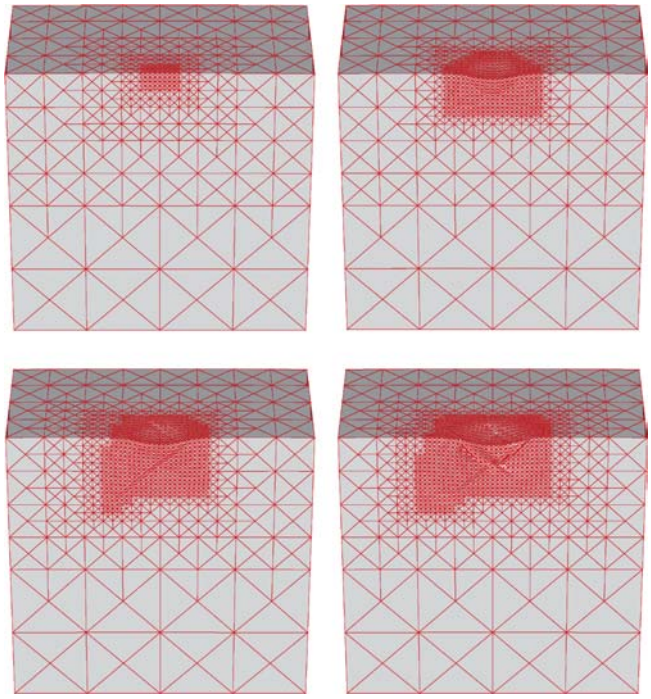

Fig. 15. Cross-sectional view of the single crystal: Adaptive mesh refinement during indentation simulation ensures that dislocations can expand and move into the bulk of the material. Sequence from top left to bottom right.

where vectors $\boldsymbol{r}_i$ and $\boldsymbol{r}_{-i}$ correspond to the six pairs of next neighbours lying at opposite sites w.r.t. the considered atom in the lattice. By definition, the centro symmetry parameter is zero for an atom in the bulk of a perfect material subject to purely homogeneous elastic deformations. The deviation of P from zero therefore measures the strength of disturbed centro symmetry at a lattice site.

The dislocation microstructure after the force-drop is shown in Fig. 16. The QC solution showing four dislocation loops slipping on {111} planes is in good agreement with lattice statics.

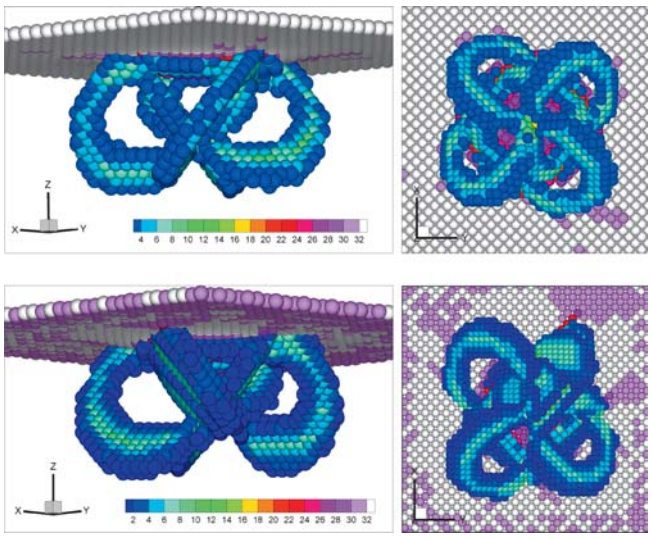

Fig. 16. Dislocation microstructure visualised by centro symmetry parameter $P \geq 2$ Å^2 for (top) lattice statics simulation and for (bottom) CQC-E.

5. Conclusions

In this contribution we have presented a comparative synopsis of different versions of the QC method and have underlined the assumptions and simplifications made with the corresponding approximation errors. Numerical errors must be estimated and reduced by appropriate means to reasonably defined tolerances, which is a standard task of numerical mathematics. As underpinned in the two benchmark problems, the question *what is accurate enough?* should be directly connected to those physical phenomena and processes that are of main interest and hence are to be simulated with high fidelity. In the example with the dipole of Lomer dislocation, the main objective of tracking the dislocation motion was captured by both QC-versions with reasonable accuracy if the dislocations could move within a sufficiently wide strip of fully atomistic resolution. The 3D nanoindentation simulations have shown the unique property of the cluster-based fully nonlocal QC to account for free surface effects as opposed to the QC version based on the CBR. Moreover, the cluster-based QC has proved its potential to reduce the prohibitive computational costs of fully atomistic resolution while faithfully simulating the material's response in all relevant aspects.

The author would like to acknowledge the financial support from the industrial sponsors of ICAMS, ThyssenKrupp Steel AG, Salzgitter Mannesmann Forschung GmbH, Robert Bosch GmbH, Bayer Materials Science AG and Bayer Technology Services GmbH, Benteler AG and the state of North-Rhine Westphalia.

References

[1] J. Fish, M.A. Nuggehally, M.S. Shephard, C.R. Picu, S. Badia, M.L. Parks, M. Gunzburger: Comp. Meth. Appl. Mech. Eng. 196 (2007) 4548–4560. DOI:10.1016/j.cma.2007.05.020
[2] S. Kohlhoff, P. Gumbsch, H.F. Fischmeister: Phil. Mag. A 64 (1991) 851–878. DOI:10.1080/01418619108213953
[3] R.E. Rudd, J.Q. Broughton: Phys. Status Solidi B 217 (2000) 251–291. DOI:10.1002/(SICI)1521-3951(200001)217:13.0.CO;2-A
[4] L.E. Shilkrot, R.E. Miller, W.A. Curtin: J. Mech. Phys. Solids 52 (2004) 755–787. DOI:10.1016/j.jmps.2003.09.023
[5] G.J. Wagner, W.K. Liu: J. Comp. Phys. 190 (2003) 249–274. DOI:10.1016/S0021-9991(03)00273-0
[6] W.A. Curtin, R.E. Miller: Model. Simul. Mater. Sci. Eng. 11 (2003) R33–R68. DOI:10.1088/0965-0393/11/3/201
[7] R.E. Miller, E.B. Tadmor: Simul. Mater. Sci. Eng. 17 (2009) 1–51. DOI:10.1088/0965-0393/17/5/053001
[8] E.B. Tadmor, M. Ortiz, R. Phillips: Phil. Mag. A 73 (1996) 1529–1563. DOI:10.1080/01418619608243000
[9] E.B. Tadmor, R. Phillips, M. Ortiz: Langmuir 12 (1996) 4529–4534. DOI:10.1021/la9508912
[10] V.B. Shenoy, R. Miller, E.B. Tadmor, D. Rodney, R. Phillips, M. Ortiz: J. Mech. Phys. Solids 47 (1999) 611–642. DOI:10.1016/S0022-5096(98)00051-9
[11] J. Knap, M. Ortiz: J. Mech. Phys. Solids 49 (2001) 1899–1923. DOI:10.1016/S0022-5096(01)00034-5
[12] B. Eidel, A. Stukowski: J. Mech. Phys. Solids 57 (1) (2009) 87–108. DOI:10.1016/j.jmps.2008.09.017
[13] M. Born, K. Huang: Dynamical Theory of Crystal Lattices, O.U. Press (Ed.), Oxford University Press, (1998).
[14] J.L. Ericksen, in: M. Gurtin (Ed.), Phase Transformations and Material Instabilities in Solids, The Cauchy–Born hypothesis for crystals, Academic Press (1984) 61–77.
[15] G. Zanzotto: Acta Crystallogr. Sect. A 52 (1996) 839–849. DOI:10.1107/S0108767396006654
[16] W. E, J. Lu, J. Yang: Phys. Rev. B 74 (2006) 214115. DOI:10.1103/PhysRevB.74.214115
[17] G. Friesecke, F. Theil: J. Nonlinear Sci. 12 (2002) 445–478. DOI:10.1007/s00332-002-0495-z
[18] R. Sunyk, P. Steinmann: Int. J. Solids Struct. 40 (2003) 6877–6896. DOI:10.1016/j.ijsolstr.2003.07.001
[19] T. Shimokawa, J.J. Mortensen, J. Schiotz, K.W. Jacobsen: Phys. Rev. B 69 (2004) 214104. DOI:10.1103/PhysRevB.69.214104
[20] R.E. Miller, E.B. Tadmor: J. Comput-Aided Mater. Des. 9 (2002) 203–239. DOI:10.1023/A:1026098010127
[21] C.L. Kelchner, S.J. Plimpton, J.C. Hamilton: Phys. Rev. B 58 (1998) 11085–11088. DOI:10.1103/PhysRevB.58.11085

(Received September 3, 2009; accepted September 17, 2009)

Bibliography

DOI 10.3139/146.110208
Int. J. Mat. Res. (formerly Z. Metallkd.)
100 (2009) 11; page 1503–1512

ISSN 1862-5282

Correspondence address

Dr. Bernhard Eidel
ICAMS, Ruhr-Universität Bochum
Stiepeler Str. 129, D-44801 Bochum, Germany
Tel.: +49 234 32 29380
Fax: +49 234 32 29380
E-mail: bernhard.eidel@rub.de